



# Nature of Magnetic Holes above Ion Scales: A Mixture of Stable Slow Magnetosonic and Unstable Mirror Modes in a Double-polytropic Scenario?

Lei Zhang<sup>1,2</sup>, Jiansen He<sup>2</sup>, Jinsong Zhao<sup>3</sup>, Shuo Yao<sup>4</sup>, and Xueshang Feng<sup>1</sup>

<sup>1</sup> SIGMA Space Weather Group, National Space Sciences Center, Chinese Academy of Sciences, Beijing, 100190, People's Republic of China

<sup>2</sup> School of Earth And Space Sciences, Peking University, Beijing, 100871, People's Republic of China; [jshept@pku.edu.cn](mailto:jshept@pku.edu.cn)

<sup>3</sup> Purple Mountain Observatory, Chinese Academy of Sciences, Nanjing, 210008, People's Republic of China

<sup>4</sup> School of Geophysics and Information Technology, China University of Geosciences (Beijing), 100083, People's Republic of China

Received 2018 March 23; revised 2018 June 26; accepted 2018 July 16; published 2018 August 29

## Abstract

Magnetic holes are common features with a prominent dip of magnetic field strength in space plasma turbulence. As to their nature, there exists a dispute of explanations among discontinuities, magnetic reconnection, solitons, kinetic-scale electron vortexes, slow waves, and mirror-mode instability. As magnetic holes are often accompanied by thermal anisotropy, at magnetohydrodynamic scales double-polytropic equations can serve as an appropriate description. The reason for the long-lasting dispute lies in the fact that both mirror-mode structures and oblique slow-mode waves are characterized with anticorrelation between plasma density (or temperature) and magnetic field strength, which, as often used in preceding works, is also the characteristic feature of magnetic holes. Therefore, to finally and unambiguously diagnose the nature of magnetic holes above ion scales, we propose to resort to other features, among which  $v_{\parallel}$  and its phase relation with  $|B|$  and  $n$  behave differently between mirror-mode structures and slow-mode waves. Herewith we establish a model with superposition of both slow and mirror modes to reproduce the observed types of behaviors ( $n$ ,  $v_{\parallel}$ ,  $|B|$ ,  $T_{\parallel}$ ,  $T_{\perp}$ ). This model inspires new understanding of the nature of magnetic holes: the magnetic hole in reality is not solely contributed by only one mode, but a mixture of the two modes with an adjustable amplitude ratio.

**Key words:** solar wind – turbulence – waves

## 1. Introduction

Magnetic holes are regions with low magnetic fields in space plasma (Turner et al. 1977; Burlaga & Lemaire 1978; Xiao et al. 2010). They are often accompanied by hotter, denser plasma, i.e., anticorrelations between magnetic field strength and temperature and density. They appear in the solar wind (Winterhalter et al. 1994), in the heliosheath (Burlaga et al. 2006), and in magnetospheres of planets such as Earth (e.g., Huang et al. 2017a), Mercury (Karlsson et al. 2016), and Venus (Futaana et al. 2017). They also come in both larger MHD (Strumik et al. 2011; Grib & Leora 2015) and kinetic (Sundberg et al. 2015; Gershman et al. 2016) scales.

Magnetic holes are also essential parts in space plasma turbulence (Tu & Marsch 1995; Bruno & Carbone 2013) and are often associated with coherent structures (Burlaga & Ness 2009; Yang et al. 2017). Magnetic holes share some features with discontinuities and/or intermittency (e.g., Grib & Leora 2015). Meanwhile, in compressible turbulence, the existence of slow waves has been identified with observational data (Howes et al. 2012; Yao et al. 2013a; He et al. 2015; Verscharen et al. 2017) and numerical simulations (Cho & Lazarian 2003). Polarization of oblique slow waves guarantees an anticorrelation between magnetic field strength and plasma density or temperature (see Hau & Sonnerup 1993, for a treatise in thermal-anisotropic cases), so slow-mode waves are closely related to pressure-balanced structures (e.g., Yao et al. 2013a) and magnetic holes.

Space plasma often shows thermal anisotropy where the plasma has different temperatures along and perpendicular to the magnetic field, and hence double-polytropic MHD models provide a more specific description. The models (see Equations 1(c) and (d)) allow for two types of instabilities:

fire-hose and mirror modes. They are also known in connection with space plasma turbulence (Maruca et al. 2011; Osman et al. 2012). The critical conditions are distinguished via the parameter  $A = T_{\perp}/T_{\parallel}$ . If critical conditions are met, when  $A < 1$ , fire-hose instability may arise; when  $A > 1$ , mirror-mode instability will arise (Hau & Wang 2007). The conditions depend on  $A$ ,  $\beta_{\parallel}$ , and also  $\theta(\mathbf{k})$ , defined as the angle between the background magnetic field  $\mathbf{B}_0$  and a given  $\mathbf{k}$ . Mirror mode also features an anticorrelation between  $B$  and  $n$  (Yao et al. 2013b). These properties allow a wave packet to contain both slow waves and mirror modes in the same plasma and to produce the anticorrelation between  $B$  and  $n$ .

In such complicated environments, the natures of magnetic holes are variously explained. The explanations have been focused on discontinuities (Tsurutani et al. 2002a, 2002b; Grib & Leora 2015), magnetic reconnection (Zurbuchen et al. 2001), solitons (Stasiewicz 2004; Burlaga & Ness 2011; Strumik et al. 2011; Ji et al. 2014; Wheeler et al. 2015; Yao et al. 2017), electron vortexes (Haynes et al. 2015; Huang et al. 2017a, 2017b), slow waves (Baumgärtel et al. 2003; Perrone et al. 2016), and mirror mode (Zhang et al. 2008; Shi et al. 2009; Tsurutani et al. 2010, 2011; Sun et al. 2012; Tsubouchi 2012). For solitons, the models should contain additional terms in comparison to common MHD equations, such as Hall (Strumik et al. 2011) or nonlinear convection terms (Ji et al. 2014), or even use derivative nonlinear Schrödinger equations (Wheeler et al. 2015). For slow waves, previous research commonly concentrated on the anticorrelation between  $B$  and  $n$ , rather than the behaviors of  $B_{\parallel}$  and  $v_{\parallel}$ . As to the behavior of  $v_{\parallel}$ , mirror mode only allows oscillations of  $v_{\parallel}$  to stay ahead of  $B_{\parallel}$  with a phase difference of  $\pi/2$ . However,  $v_{\parallel}$  in realistic magnetic holes behaves variously (see Section 2). Meanwhile, it is also meaningful to check the behavior of wave packets superposed

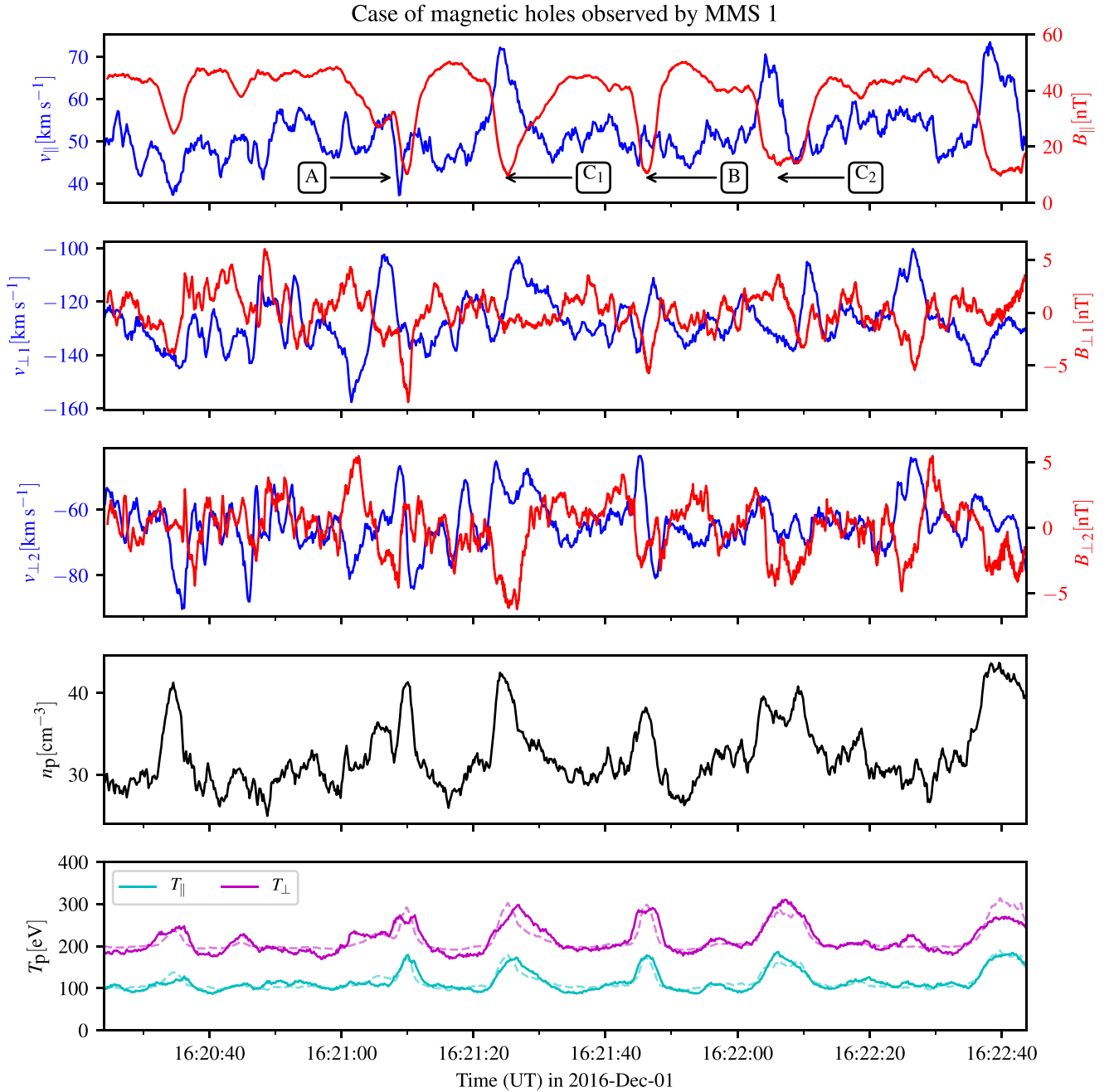


**Figure 1.** Example of magnetic holes observed by *MMS* Satellite 1. Typical cases of magnetic holes are labeled as A, B, C<sub>1</sub>, and C<sub>2</sub>. Fitted temperatures are also plotted with dashed lines.

by both unstable and stable modes, shedding new light on the dispute over the nature of magnetic holes above ion scales.

To investigate the nature of magnetic holes and their relationships with slow and mirror modes, herewith we present a simplified scenario of superposition of the two modes in double-polytropic MHD descriptions. Here we regard the types of behavior of  $v_{\parallel}$  (compared with  $B_{\parallel}$ ) as a vital sign of our proposed scenario. Section 1 introduces the topics of magnetic holes, thermal anisotropy, and slow waves and instabilities. Section 2 shows a case of magnetic holes observed in space plasma. Section 3 overviews the solution of thermal-anisotropic slow and mirror modes and illustrates the properties of these

modes. Section 4 shows our model result of superposition of slow and mirror modes. Section 5 summarizes our research and discusses further issues.

## 2. A Case of Magnetic Holes

As an in situ observed case of magnetic holes, we present the data in Figure 1. For protons, we plot their number density  $n_p$  and their parallel and perpendicular temperatures ( $T_{\parallel}$ ,  $T_{\perp}$ ). Their bulk velocities are also plotted along with corresponding magnetic field components. All the directions are relative to the mean field  $\langle \mathbf{B} \rangle$ , and the axes of the two perpendicular directions

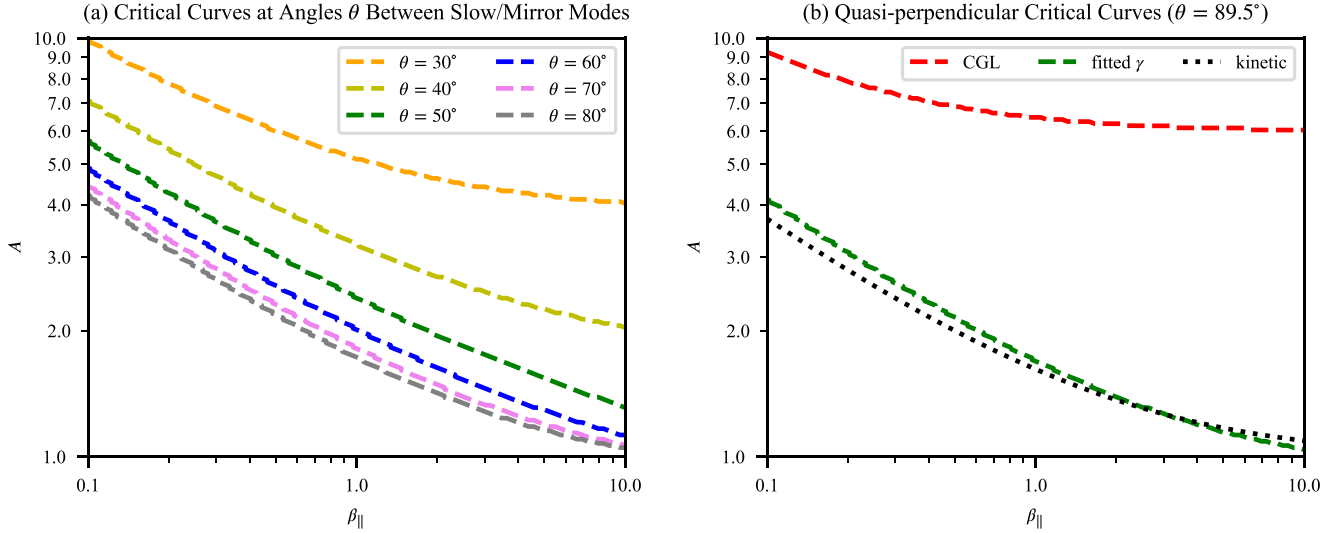


**Figure 2.** Critical curves of mirror instability: (a) for different  $\theta$  when  $(\gamma_{\parallel}, \gamma_{\perp}) = (1.33, 0.69)$ ; (b) comparison of our fitted polytropic, classical CGL, and kinetic models.

are assigned arbitrarily, as long as the three directions form a right-handed orthogonal coordinate triad. The data are obtained from the Flux Gate Magnetometer and Fast Plasma Investigation (FPI) on board *Magnetospheric MultiScale (MMS)* Spacecraft 1 between 16:20:24 to 16:22:43 UT, 2016 December 1. The samplings are taken from plasma in Earth's magnetosheath turbulence. Here our methods and results are rather general for space plasma. Except for several short spiky features, the plasma background is calm. Hence, one assumes that  $B_0 \approx 40$  nT,  $n \approx 30 \text{ cm}^{-3}$ ,  $T_{\parallel} \approx 100$  eV, and  $T_{\perp} \approx 200$  eV, so that the parameters are calculated as  $A = T_{\perp}/T_{\parallel} \approx 2.0$ ,  $\beta_{\parallel} \approx 1.5$ , and  $\beta_{\perp} \approx 3.0$ .

The spiky features uniformly share the following features: they have lower  $|B|$ , denser  $n$ , and increased  $T$ . Spikes of these quantities are almost arranged in time, suggesting the same phase. The significant drop in  $|B|$  characterizes the troughs as magnetic holes. Increased  $n$  and  $T$  accompany the drop of  $|B|$ , forming an anticorrelation. Meanwhile, the behavior of  $v_{\parallel}$  is vastly varying. It can be categorized as labeled in Figure 1. Type A has a positive correlation of  $v_{\parallel}$  and  $B_{\parallel}$ . Type B does not show obvious features of  $v_{\parallel}$ . Type C shows an anticorrelation between  $v_{\parallel}$  and  $B_{\parallel}$ , and it has two subtypes: in subtype  $C_1$ , the bumps of  $v_{\parallel}$  almost coincide with the troughs of  $B_{\parallel}$ ; in subtype  $C_2$ , the width of the spike of  $v_{\parallel}$  is almost half of the width of the trough. The typical sizes of magnetic holes are estimated as  $\sim 3$  s, or equivalently 600 km here, and the gyro-radius of protons is  $\sim 30$  km. Hence, the scales of magnetic holes are well above ion scales, and fluid-like descriptions are appropriate.

### 3. Stable and Unstable Modes in the Double-polytropic Scenario

The double-polytropic scenario describes plasma in the following MHD form (see Hau & Wang 2007):

$$\frac{d\rho_i}{dt} + \nabla \cdot (\rho_i \mathbf{v}_i) = 0, \quad (1a)$$

$$\rho_i \cdot \frac{d\mathbf{v}_i}{dt} = -\nabla \cdot (\mathbf{P}_i + \mathbf{P}_e) + \mathbf{j} \times \mathbf{B}, \quad (1b)$$

$$\frac{p_{\perp,s}}{\rho_s B^{\gamma_{\perp,s}-1}} = \text{Const.}, \quad (1c)$$

$$\frac{p_{\parallel,s} B^{\gamma_{\parallel,s}-1}}{\rho_s^{\gamma_{\parallel,s}}} = \text{Const.}, \quad (1d)$$

$$\frac{\partial \mathbf{B}}{\partial t} = \nabla \times (\mathbf{v}_i \times \mathbf{B}), \quad (1e)$$

$$\nabla \times \mathbf{B} = \mathbf{j}. \quad (1f)$$

Here  $d/dt$  denotes material derivatives defined as  $d/dt = \partial/\partial t + \mathbf{v} \cdot \nabla$ . The  $\gamma$  represents polytropical indices, and  $s$  represents species of particles, here assumed as electrons ( $e$ ) and protons ( $i$ ). Here the equations are normalized, and  $\mu_0$  does not appear in the equations. The results below are also presented in normalized forms. If one hopes to relate to the aforementioned observations, one might as well take  $\rho_0 = 5 \times 10^{-20} \text{ kg m}^{-3}$ ,  $B_0 = 40$  nT, and  $v_0 = 160 \text{ km s}^{-1}$ . The  $v_0$  is taken as Alfvén speed, so that  $\mu_0$  does not appear in the normalized form.

The set of equations only introduced thermal anisotropy (see Equations 1(d) and (c)). For any species  $s$ , the thermal pressure tensor  $\mathbf{P}_s = p_{\parallel,s} \hat{\mathbf{B}}\hat{\mathbf{B}} + (p_{\perp,s} - p_{\parallel,s})\mathbf{I}$ , where the parallel and perpendicular pressures  $p_{\parallel,\perp}$  are scalars. One should note that the derivatives of  $\mathbf{P}$  contain two parts: changes of physical quantities and changes of local field directions (Barbara 1967). When corresponding values for electrons and ions are equal,  $\gamma_{\parallel} = 3$ , and  $\gamma_{\perp} = 2$ , the equations are reduced to familiar CGL equations given by Chew et al. (1956). However, in real plasma the parameters  $\gamma$  can be empirically fitted according to the Hau et al. (1993) methods (essentially a linear fit when  $p$ ,  $\rho$ , and  $B$  are given), and in our case we got  $\gamma_{\parallel} \approx 1.33 \pm 0.01$  and  $\gamma_{\perp} \approx 0.69 \pm 0.01$ . We will use these values for our numerical solutions.

Therefore, after linearization, the plane wave mode with  $(\omega, \mathbf{k})$  should fit

$$\begin{pmatrix}
0 & B_0^2 k_{\parallel} v_A & B_0^2 k_{\perp} v_A & 0 & 0 & 0 & 0 & 0 & 0 & 0 & 0 \\
0 & 0 & 0 & 0 & 0 & \frac{k_{\perp} \Delta\beta}{2B_0 v_A} & 0 & \frac{k_{\parallel}}{B_0^2 v_A} & \frac{k_{\parallel}}{B_0^2 v_A} & 0 & 0 \\
0 & 0 & 0 & 0 & \frac{k_{\perp}}{B_0 v_A} & \frac{k_{\parallel} \cdot (\Delta\beta - 2)}{2B_0 v_A} & 0 & 0 & 0 & \frac{k_{\perp}}{B_0^2 v_A} & \frac{k_{\perp}}{B_0^2 v_A} \\
0 & 0 & 0 & 0 & 0 & 0 & \frac{k_{\parallel} \cdot (\Delta\beta - 2)}{2B_0 v_A} & 0 & 0 & 0 & 0 \\
0 & 0 & B_0 k_{\perp} & 0 & 0 & 0 & 0 & 0 & 0 & 0 & 0 \\
0 & 0 & -B_0 k_{\parallel} & 0 & 0 & 0 & 0 & 0 & 0 & 0 & 0 \\
0 & 0 & 0 & -B_0 k_{\parallel} & 0 & 0 & 0 & 0 & 0 & 0 & 0 \\
\frac{B_0^2 \gamma_{e\parallel} k_{\parallel} / \beta_{e\parallel}}{2} & \frac{B_0^2 \beta_{e\parallel} k_{\perp}}{2} & 0 & 0 & 0 & 0 & 0 & 0 & 0 & 0 & 0 \\
\frac{B_0^2 \gamma_{i\parallel} k_{\parallel} / \beta_{i\parallel}}{2} & \frac{B_0^2 \beta_{i\parallel} k_{\perp}}{2} & 0 & 0 & 0 & 0 & 0 & 0 & 0 & 0 & 0 \\
\frac{B_0^2 \beta_{e\perp} k_{\parallel}}{2} & \frac{B_0^2 \gamma_{e\perp} k_{\perp} / \beta_{e\perp}}{2} & 0 & 0 & 0 & 0 & 0 & 0 & 0 & 0 & 0 \\
\frac{B_0^2 \beta_{i\perp} k_{\parallel}}{2} & \frac{B_0^2 \gamma_{i\perp} k_{\perp} / \beta_{i\perp}}{2} & 0 & 0 & 0 & 0 & 0 & 0 & 0 & 0 & 0
\end{pmatrix} \cdot \begin{pmatrix} \delta\rho \\ \delta v_{\parallel} \\ \delta v_2 \\ \delta v_3 \\ \delta B_{\parallel} \\ \delta B_2 \\ \delta B_3 \\ p_{e\parallel} \\ p_{i\parallel} \\ p_{e\perp} \\ p_{i\perp} \end{pmatrix} = \omega \begin{pmatrix} \delta\rho \\ \delta v_{\parallel} \\ \delta v_2 \\ \delta v_3 \\ \delta B_{\parallel} \\ \delta B_2 \\ \delta B_3 \\ p_{e\parallel} \\ p_{i\parallel} \\ p_{e\perp} \\ p_{i\perp} \end{pmatrix}, \quad (2)$$

with  $\Delta\beta$  defined as  $\sum_s(\beta_{s\parallel} - \beta_{s\perp})$ , and  $v_A$  as  $B_0/\sqrt{\rho_i}$ . Equation (2) is an eigensystem equation. The dispersion relations come from its eigenvalues, and the polarization from eigenvectors.

Suppose that  $\mathbf{k} = (k_{\parallel} = k \cos \theta, k_{\perp} = k \sin \theta, 0)$  are real-valued. Here we consider only slow and mirror modes (since  $A > 1$ ). The solved  $\omega$  can be real or imaginary, which respectively correspond to stable and unstable modes. If there is instability, we take the eigenmode with  $\text{Im } \omega > 0$  and label it as the mirror mode; otherwise, we find the mode with the least positive absolute value of phase velocity and label it as the slow mode. The eigensystem has a noteworthy property: if instability is excited, the  $\omega$  is purely imaginary; hence, there will be differences of phases between oscillations of the variables, since a real-valued matrix cannot have a real-valued eigenvector corresponding to an imaginary eigenvalue.

The eigensystem can indeed be solved algebraically; however, since the formulae of solving roots are cumbersome, we seek numerical solutions instead. In our simplified model, we also take  $\gamma_{i\parallel} = \gamma_{e\parallel}$ ,  $\gamma_{i\perp} = \gamma_{e\perp}$ ,  $\beta_{i\parallel} = \beta_{e\parallel}$ , and  $\beta_{i\perp} = \beta_{e\perp}$ . For a given  $\theta$ , there exists a critical curve for mirror modes to be excited (see Figure 2 for examples). If  $\beta_{\parallel}$  or  $A$  is larger

(“upper right”), there will be unstable mirror modes; if the parameters are smaller (“lower left”), slow-mode waves will exist instead. For example, the critical curve of  $\theta = 52^\circ 8'$  passes  $(\beta_{\parallel}, A) = (1.5, 2.0)$  as in our case. With this set of  $(\beta_{\parallel}, A)$ , the slow magnetosonic mode with  $\theta = 50^\circ$  is stable, and its counterpart with  $\theta = 53^\circ$  becomes mirror-mode instability. We plotted thresholds of quasi-perpendicular mirror mode in our model with CGL and kinetic (Tajiri 1967) counterparts in panel (b) as well. Compared with CGL modes, our thresholds are much closer to the kinetic theory’s.

To visualize and compare their polarization, we plot  $\rho$ ,  $\mathbf{B}$ , and  $\mathbf{v}$  in the plane decided by  $\mathbf{B}_0$  and  $\mathbf{k}$  as shown in Figure 3. The  $z$ -axis is the direction of the background field. The  $x$ -axis is located so that  $\mathbf{k}$  lies in the  $xz$ -plane. Since the angle  $\theta$  is rather close, the profiles resemble each other rather closely, only with a subtle but essential difference: in the stable case, the maxima of velocity appear at the extremes of  $\rho$ , and everything has the same phase; in the mirror-mode instability, the maxima of velocity appear when  $\rho$  has no oscillations, indicating a phase difference of  $\pi/2$ .

To illustrate this characteristic in a fashion closer to in situ measurements, we used a virtual probe to sample both fields



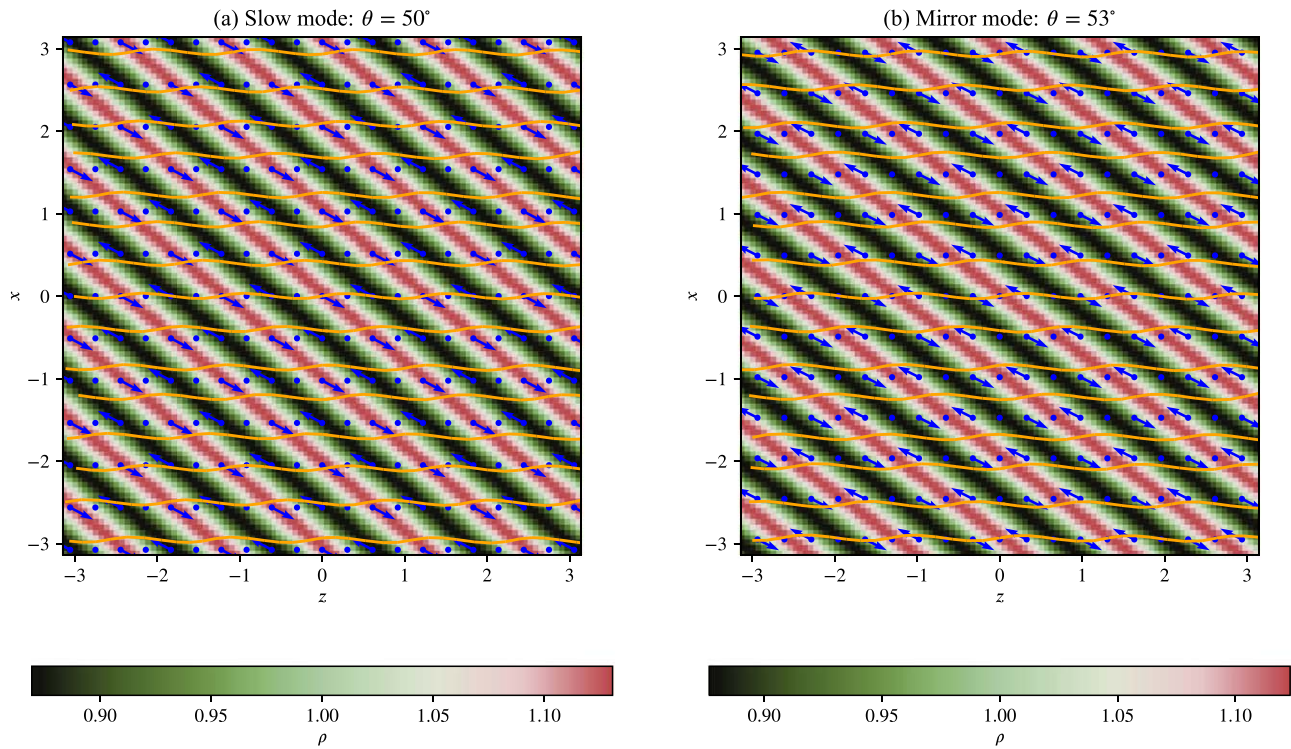


**Figure 3.** Comparison of polarizations between (a) slow and (b) mirror modes. The colors display oscillation of  $\rho$ . The orange curves plot magnetic field lines, and the blue arrows show velocities at the blue points.

(see Figure 4). Here the probe starts at (0, 0) and moves along  $B_0$  at a speed of 1. The initial amplitudes are different from those in Figure 3. Besides the growth of oscillations in the case of mirror instability, the phase differences between oscillations are also distinct between the stable and unstable modes. Here one clearly sees in the case of instability that the phase of  $v$  stays  $\pi/2$  ahead of other quantities.

The common features of the two modes are also noteworthy:  $B$ ,  $\rho$ , and  $p$  all oscillate in phase, with a positive-correlated  $\rho$  and  $p$  and negative correlation between  $B$  and  $\rho$  (or  $p$ ). Such relationships conform with observed properties of magnetic holes. Therefore, all the features justify both modes as suitable building blocks of a superposed wave-packet model of magnetic holes.

#### 4. Superposition of the Stable and Unstable Modes

However, a closer inspection of observed cases shows a variety of phase differences between the velocity and magnetic field signals. To explain the irregular phase difference, we assume a linear superposition of slow and mirror modes. For example, we shall start with a rectangular wave-like magnetic hole, resembling the one at  $\sim 16:22:10$  UT in Figure 1.

For a rectangular wave

$$a(x) = \begin{cases} 1, & \text{if } x \bmod X_1 \in [0, X_2/2] \cup [X_1 - X_2/2, X_1), \\ 0, & \text{otherwise,} \end{cases} \quad (3)$$

with  $0 < X_2 < X_1$ , where  $X_1$  is the period and  $X_2$  is the pulse duration. Its cosine Fourier transform reads

$$a(x) = C \sum_{n=1}^{\infty} A_n \cos(k_n x), \quad (4a)$$

$$A_n = \frac{X_1}{n\pi} \sin \frac{N\pi X_2}{X_1}, \quad (4b)$$

$$k_n = \frac{2n\pi}{X_1}, \quad (4c)$$

where  $C$  is a constant factor. If only the first term is considered, we get a sinusoidal wave. If the infinity sum were taken, we would get a rectangular wave. Here we take the first 11 terms to get a waveform between these two types, and we set the ratio  $X_2/X_1 = 1/8$ . In actual waves, here  $x$  refers to phase, i.e.,  $\mathbf{k} \cdot \mathbf{x} - \omega t$ .

For an  $A_n$ , we set a pair of one slow mode and one mirror mode. The amplitudes of both modes are set as a constant; this value controls the polarization and their differences of phases. However, in actual oscillations there are many quantities rather than a single  $A_n$ . For the superposition, we take  $\delta p_{e\perp}$  to represent amplitudes of a wave mode; the amplitudes of other quantities are set according to polarization. Here we choose a ratio of amplitude slow:mirror = 1:4. The phase difference of  $\delta p_{e\perp}$  between both modes, denoted as  $\Delta\phi$  (i.e., in a pair,  $\delta p_{e\perp}^{\text{mirror}} = 4 \exp(-i\Delta\phi) \delta p_{e\perp}^{\text{slow}}$ ), is set differently for the three types of correlations between  $v_{\parallel}$  and  $B_{\parallel}$ . Here the differences are respectively  $212^\circ$ ,  $270^\circ$ ,  $305^\circ$ , and  $99^\circ$ . Therefore, we have a wave packet of 11 pairs of slow and mirror modes. As the growth of instabilities is restricted by the plasma (e.g., Maruca et al. 2011), we remove the temporal growth part of instabilities in this superposed wave packet and only use the phase difference of slow modes for the virtual probe to represent a “quasi-static” state. We also choose the parameters of samples differently, in that the velocity of the virtual sampler is  $(V_{\parallel}, V_{\perp}) = (5, 0)$  instead. This velocity is not vital, so we do not set it according to the ratio of the bulk plasma speed to the Alfvén speed in the observational case.

## Waveforms of Pure Modes Sampled Virtually

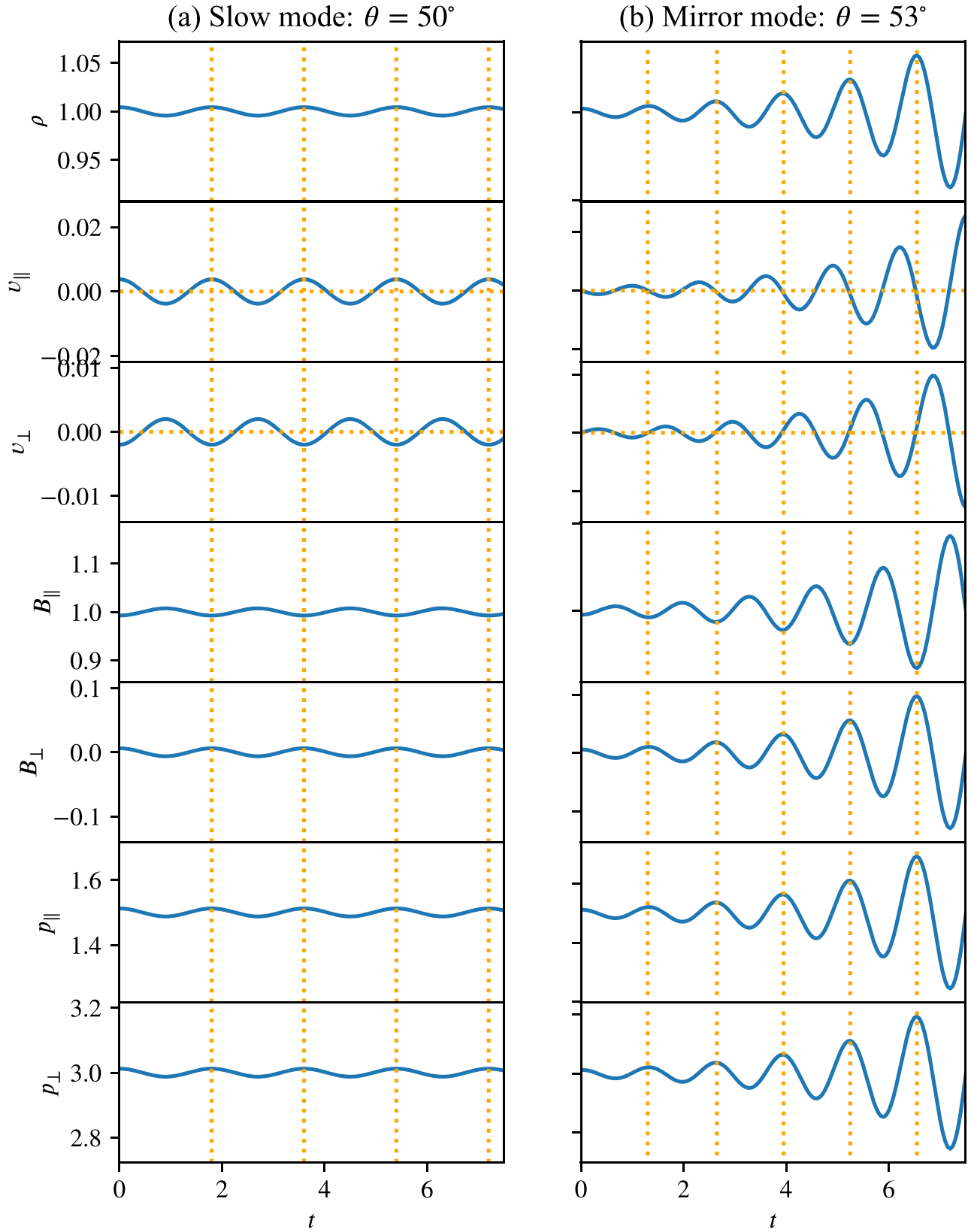


**Figure 4.** Comparison of pure (a) slow and (b) mirror modes sampled virtually. For reference, the local maxima of  $\rho$  are marked with vertical dotted lines;  $v_{\parallel} = 0$  and  $v_{\perp} = 0$ , with horizontal dotted lines.

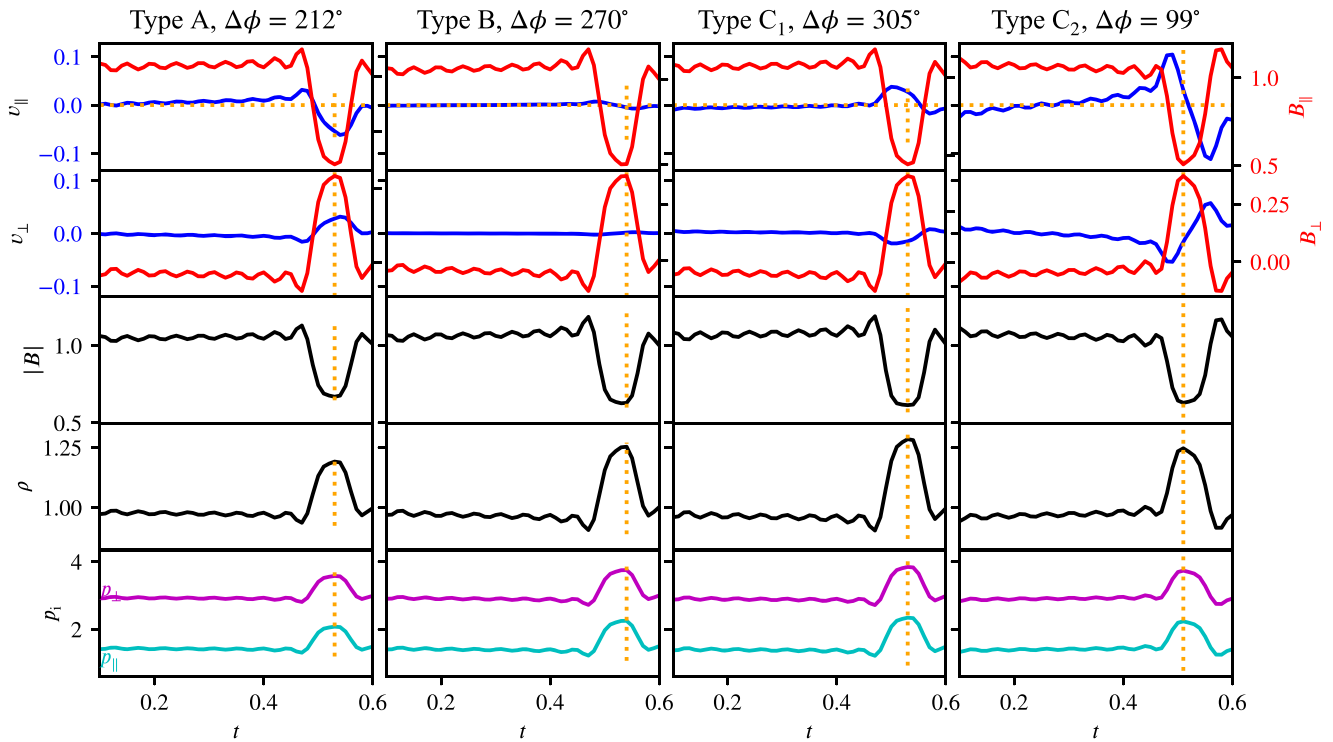


**Figure 5.** Mixture of stable and unstable modes. The columns exhibit different types of mixture distinguished by  $\Delta\phi$ . The quantities are plotted as in Figure 1, but with  $p_i$  instead of  $T_i$ . For reference, the local maxima of  $\rho$  are marked with vertical dotted lines;  $v_{||} = 0$  and  $v_{\perp} = 0$ , with horizontal dotted lines.

The superposed profile is plotted in Figure 5. Here the anticorrelations between  $|B|$  and  $\rho$  (or  $p$ ) are reproduced. As to correlations between  $B_{||}$  and  $v_{||}$ , the types are also reproduced: positive correlation for type A, insignificant oscillations of  $v_{||}$  for type B, and typical anticorrelation for type C, with their characteristic relations for subtypes  $C_1$  and  $C_2$ . In this way, the main features of different types of magnetic holes are reproduced as a superposition of slow and mirror modes.

## 5. Summary and Discussion

In this paper, we have provided an explanation of the nature of magnetic holes as a combination of slow magnetosonic and mirror modes. The behaviors of  $v_{||}$  are categorized according to their shape and correlation with the density. We have established a model of magnetic holes as a superposition of slow and mirror modes, and the differences of phases largely affect the profiles of  $v_{||}$ , meanwhile keeping the essential features of decreased  $B_{||}$  and  $|B|$  and increased  $\rho$  and  $p$ . All the types of magnetic holes are reproduced within the uniform settings of plasma and wave packets except for different phases between the two modes. These results may reveal the important roles played by both slow and mirror modes in magnetic holes and clear up complexity in behaviors of  $v$  therein.

Besides the success in reproducing the various behaviors of magnetic holes, we must acknowledge limitations in this work. The double-polytropic MHD model does not involve kinetic procedures (e.g., Hau & Wang 2007), and finer models should involve kinetic features (e.g., Gershman et al. 2016; Huang et al. 2017a) to describe magnetic holes at kinetic scales. Otherwise, the Hall term and soliton theory could also be introduced in this model instead of simple rectangular waves to provide more self-contained descriptions; nonlinear processes can also be considered more self-contained as compared to this

linearized method presented above. However, as the data give  $|\mathbf{j} \times \mathbf{B}/(n_i e)| \sim 0.1|\mathbf{v}_i \times \mathbf{B}|$ , the Hall term could be regarded as marginal in our simplified model. Its introduction will partly change the phase relations (Stasiewicz 2004, 2005). On the other hand, we compared mirror modes in our simplified model with those in a kinetic model by the New Hampshire Dispersion Relation Solver (NHDS; Verscharen & Chandran 2018), and we found essentially the same phase differences between  $\delta n$ ,  $\delta v_{||}$ , and  $\delta B_{||}$ . This justifies our simplified polytropic model.

As to the modeling of the phenomena, we have not considered the geometric features (e.g., sizes and depths). If all the multispacecraft data are used, some reconstructions may be conducted to provide more geometrically precise descriptions to compare with observations (e.g., Sundberg et al. 2015). Also, the  $\theta$  for mirror mode could be better fitted. If the spectra before excitation of mirror-mode instability were uniform, modes with larger theta would dominate owing to larger growth rate, instead of oblique wavevectors chosen in our simplified model. MVA results on  $\delta B$ , which gives a  $\theta \sim 87^\circ$ , might suggest this point of view. However, since 3D turbulence spectra remain largely unknown, we could not yet make any practical assumptions on dominating mirror modes. Some magnetic holes observed in situ and interpreted with mirror modes, e.g., the case from Yao et al. (2013b) with  $\theta \sim 69^\circ$ , suggest the existence of oblique mirror modes. More practical modeling and/or fitting of  $\theta$  requires further work. Also, in order to estimate contributions of both modes and to understand the nature of magnetic holes, fitting of spacecraft observations with our model might be helpful. Some algorithms might be applied to make our model output similar to certain observations, but their physical significance still needs to be clarified further. To realize this fitting, one might consider for both the slow mode and the mirror mode (1)  $\theta$ , (2)



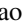

amplitudes, and (3) widths of magnetic holes. Also, the relative phase between modes matters, requiring seven parameters in total.

Finally, our simplified model does not consider temporal changes; hence, we cannot yet answer with regard to stability and life spans of magnetic holes. Such investigations also need temporal-evolving numerical models. Hence, more mechanisms, such as sharpening of waves (Tsurutani et al. 2010), and more complicated field configuration (Tsubouchi 2012) might be considered, which might lead to a self-contained temporal-evolving model to discuss the origin of magnetic holes.

This research is supported by the NSFC under contracts 41574168, 41231069, 41274172, 41474148, 41421003, 41574166, 41531073, and 41731067. J.H. is also supported by the National Young Talent Program of China. J.Z. is supported by the Youth Innovation Promotion Association CAS. The MMS data used in this work are available from the MMS Science Data Center (<http://lasp.colorado.edu/mms/sdc>). We are grateful to the referee for insightful comments that helped to further improve and clarify the paper.

*Software:* scipy (<http://www.scipy.org>), matplotlib (<http://www.matplotlib.org>).

### ORCID iDs

Lei Zhang  <https://orcid.org/0000-0003-2562-0698>  
 Jiansen He  <https://orcid.org/0000-0001-8179-417X>  
 Jinsong Zhao  <https://orcid.org/0000-0002-3859-6394>  
 Xueshang Feng  <https://orcid.org/0000-0001-8605-2159>

### References

- Barbara, A. 1967, *JPIPh*, 1, 361  
 Baumgärtel, K., Sauer, K., & Dubinin, E. 2003, *GeoRL*, 30, 1761  
 Bruno, R., & Carbone, V. 2013, *LRSP*, 10, 2  
 Burlaga, L. F., & Lemaire, J. F. 1978, *JGR*, 83, 5157  
 Burlaga, L. F., & Ness, N. F. 2009, *ApJ*, 703, 311  
 Burlaga, L. F., & Ness, N. F. 2011, *JGRA*, 116, A05102  
 Burlaga, L. F., Ness, N. F., & Acuña, M. H. 2006, *ApJ*, 642, 584  
 Chew, G. F., Goldberger, M. L., & Low, F. E. 1956, *RSPSA*, 236, 112  
 Cho, J., & Lazarian, A. 2003, *MNRAS*, 345, 325  
 Futaana, Y., Stenberg Wieser, G., Barabash, S., & Luhmann, J. G. 2017, *SSRv*, 212, 1453  
 Gershman, D. J., Dorelli, J. C., Viñas, A. F., et al. 2016, *GeoRL*, 43, 4112  
 Grib, S. A., & Leora, S. N. 2015, *Ge&Ae*, 55, 158  
 Hau, L.-N., Phan, T.-D., Sonnerup, B. U. O., & Paschmann, G. 1993, *GeoRL*, 20, 2255  
 Hau, L.-N., & Sonnerup, U. O. 1993, *GeoRL*, 20, 1763  
 Hau, L.-N., & Wang, B.-J. 2007, *NPGeo*, 14, 557  
 Haynes, C. T., Burgess, D., Camporeale, E., & Sundberg, T. 2015, *PhPI*, 22, 012309  
 He, J., Tu, C., Marsch, E., et al. 2015, *ApJL*, 813, L30  
 Howes, G. G., Bale, S. D., Klein, K. G., et al. 2012, *ApJL*, 753, L19  
 Huang, S. Y., Du, J. W., Sahraoui, F., et al. 2017a, *JGRA*, 122, 8577  
 Huang, S. Y., Sahraoui, F., Yuan, Z. G., et al. 2017b, *ApJL*, 836, L27  
 Ji, X.-F., Wang, X.-G., Sun, W.-J., et al. 2014, *JGRA*, 119, 4281  
 Karlsson, T., Liljeblad, E., Kullen, A., et al. 2016, *P&SS*, 129, 61  
 Maruca, B. A., Kasper, J. C., & Bale, S. D. 2011, *PhRvL*, 107, 201101  
 Osman, K. T., Matthaeus, W. H., Hnat, B., & Chapman, S. C. 2012, *PhRvL*, 108, 261103  
 Perrone, D., Alexandrova, O., Mangeney, A., et al. 2016, *ApJ*, 826, 196  
 Shi, Q. Q., Pu, Z. Y., Soucek, J., et al. 2009, *JGRA*, 114, A10202  
 Stasiewicz, K. 2004, *PhRvL*, 93, 125004  
 Stasiewicz, K. 2005, *JGR*, 110, A03220  
 Strumik, M., Stasiewicz, K., Cheng, C. Z., & Thidé, B. 2011, *JGRA*, 116, A07209  
 Sun, W. J., Shi, Q. Q., Fu, S. Y., et al. 2012, *AnGeo*, 30, 583  
 Sundberg, T., Burgess, D., & Haynes, C. T. 2015, *JGRA*, 120, 2600  
 Tajiri, M. 1967, *JPSJ*, 22, 1482  
 Tsubouchi, K. 2012, *JGRA*, 117, A07102  
 Tsurutani, B. T., Dasgupta, B., Galvan, C., et al. 2002a, *GeoRL*, 29, 2233  
 Tsurutani, B. T., Galvan, C., Arballo, J. K., et al. 2002b, *GeoRL*, 29, 1528  
 Tsurutani, B. T., Lakhina, G. S., Verkhoglyadova, O. P., et al. 2011, *JGRA*, 116, A02103  
 Tsurutani, B. T., Lakhina, G. S., Verkhoglyadova, O. P., Echer, E., & Guarnieri, F. L. 2010, *NPGeo*, 17, 467  
 Tu, C., & Marsch, E. 1995, *SSRv*, 73, 1  
 Turner, J. M., Burlaga, L. F., Ness, N. F., & Lemaire, J. F. 1977, *JGR*, 82, 1921  
 Verscharen, D., & Chandran, B. D. G. 2018, *RNAAS*, 2, 13  
 Verscharen, D., Chen, C. H. K., & Wicks, R. T. 2017, *ApJ*, 840, 106  
 Wheeler, H. R., Reynolds, M. A., & Hamilton, R. L. 2015, *JGRA*, 120, 1509  
 Winterhalter, D., Neugebauer, M., Goldstein, B. E., et al. 1994, *JGR*, 99, 23371  
 Xiao, T., Shi, Q. Q., Zhang, T. L., et al. 2010, *AnGeo*, 28, 1695  
 Yang, L., He, J., Tu, C., et al. 2017, *ApJ*, 836, 69  
 Yao, S., He, J., Tu, C., Wang, L., & Marsch, E. 2013a, *ApJ*, 774, 59  
 Yao, S., He, J., Tu, C., Wang, L., & Marsch, E. 2013b, *ApJ*, 776, 94  
 Yao, S. T., Wang, X. G., Shi, Q. Q., et al. 2017, *JGRA*, 122, 1990  
 Zhang, T. L., Russell, C. T., Baumjohann, W., et al. 2008, *GeoRL*, 35, L10106  
 Zurbuchen, T. H., Hefti, S., Fisk, L. A., et al. 2001, *JGR*, 106, 16001